The EMBO Journal vol.7 no.2 pp.339-343, 1988

Crystal structure of the cytokine interleukin-1β

John P.Priestle, Hans-Peter Schär[1] and Markus G.Grütter[2]

Department of Structural Biology, Biocenter, University of Basel, Klingelbergstrasse 70, CH-4056 Basel, and [1]Central Research Laboratories and [2]Pharmaceuticals Research Division, Ciba-Geigy Ltd, CH-4002 Basel, Switzerland

Communicated by J.N.Jansonius

The crystal structure of human recombinant interleukin-1β has been determined at 3.0 Å resolution by the isomorphous replacement method in conjunction with solvent flattening techniques. The model prior to refinement has a crystallographic *R*-factor of 42.3%. The structure is composed of 12 β-strands forming a complex network of hydrogen bonds. The core of the structure can best be described as a tetrahedron whose edges are each formed by two antiparallel β-strands. The interior of this structure is filled with hydrophobic side chains. There is a 3-fold repeat in the folding of the polypeptide chain. Although this folding pattern suggests gene triplication, no strong internal sequence homology between topologically corresponding residues exists. The folding topology of interleukin-1β is very similar to that described by McLachlan (1979) *J. Mol. Biol.*, 133, 557-563, for soybean trypsin inhibitor.

Key words: cytokines/interleukin-1/X-ray crystallography/protein structure

Introduction

Interleukins belong to a family of cellular mediators known as cytokines. They produce a variety of biological and physiological responses, most notably thymocyte and lymphocyte proliferation. Interleukin-1 (IL-1) has many of the activities of interleukin-2 (IL-2), but does not support the growth of IL-2-dependent lymphocyte cell lines (Mizel and Farrar, 1979). IL-1 activity has been reported in virtually all nucleated cell types. IL-1 has an effect on various types of cells and organs including proliferation of lymphocytes, epithelial cells, synovial cells, endothelial cells and fibroblasts, and increases prostaglandin activity in macrophages, brain cells, synovial cells, endothelial cells, muscle cells, chondrocytes and fibroblasts (for a review, see Oppenheim *et al.*, 1986). Two IL-1 molecules have been characterized, interleukin-1α (IL-1α) and interleukin-1β (IL-1β). Both are expressed as larger precursor molecules. The IL-1α precursor is a 31 kd protein of 271 amino acids, while the precursor of IL-1β has 269 amino acid residues. IL-1 is assumed to be a secreted protein, but lacks a signal sequence, suggesting that it may be released by some other mechanism (Gery and Lepe-Zuniga, 1983). The active IL-1α retains the 159 carboxyl-terminal residues of its precursor whereas the active IL-1β retains 153. Despite the similarity in size, function and characteristics, IL-1α and IL-1β possess only 23% amino acid sequence identity (Auron *et al.*, 1984; March *et al.*, 1985).

Human IL-1β has been cloned and expressed in *Escherichia coli* (Wingfield *et al.*, 1986). Since native IL-1β is not known to contain metal ions, carbohydrates or prosthetic groups (Kronheim *et al.*, 1985; Cameron *et al.*, 1985; Dewhirst *et al.*, 1985), the recombinant product was expected to be indistinguishable from the natural one. Biochemical characterization and *in vitro* assays of the recombinant protein (Wingfield *et al.*, 1986) support this supposition. Hydrodynamic studies of the recombinant product indicate that the protein is nearly spherical ($f/f_o = 1.09$; Wingfield *et al.*, 1986). Circular dichroism (CD) measurements of the recombinant product suggest a non-helical protein with 59% of the residues in β-sheets, the remainder consisting of random coil and/or reverse turns (Craig *et al.*, 1987). We have crystallized human recombinant IL-1β (Schär *et al.*, 1987) and report here the determination of its three-dimensional structure to 3.0 Å resolution using X-ray crystallographic techniques. The polypeptide chain folding and the model are discussed in the light of spectroscopic and hydrodynamic observations.

Results

Interpretation of the electron density map

A preliminary 5.0 Å electron density map clearly indicated that the asymmetric unit of the crystallographic unit cell contains one IL-1β molecule, implying a crystal solvent content of 63% by volume. The 3.0 Å electron density map showed that IL-1β is an all-β protein composed of 12 strands. There were, however, several main chain discontinuities in the electron density, especially at the loops between β-strands. In order to correlate the amino acid sequence with the electron density, the environment of the two binding sites of the mercurial reagent *p*-hydroxymercuribenzoate (PHMB) was investigated. The two sites are only 3.7 Å apart. These were assumed to correspond to binding to two different conformations of the same cysteine residue (Cys-8 or Cys-71). The sequences around these cysteines are very similar and almost palindromic with respect to size and shape of the side chains: Ser-Leu-Asn-Cys(8)-Thr-Leu-Arg and Tyr-Leu-Ser-Cys(71)-Val-Leu-Lys. Based on the Ser/Tyr difference, the former sequence fitted the electron density near the mercurial binding sites better. The direction of the main chain was subsequently selected on the basis of the electron density for the main chain carbonyl oxygen atoms, although this was often ambiguous. Once a starting point and the chain direction were established, and the β-strands correctly connected, it was possible to fit essentially the entire IL-1β sequence to the electron density map. Two residues at the amino-terminus and eight in loops could not be located. Figure 1 shows a representative part of the electron density map and

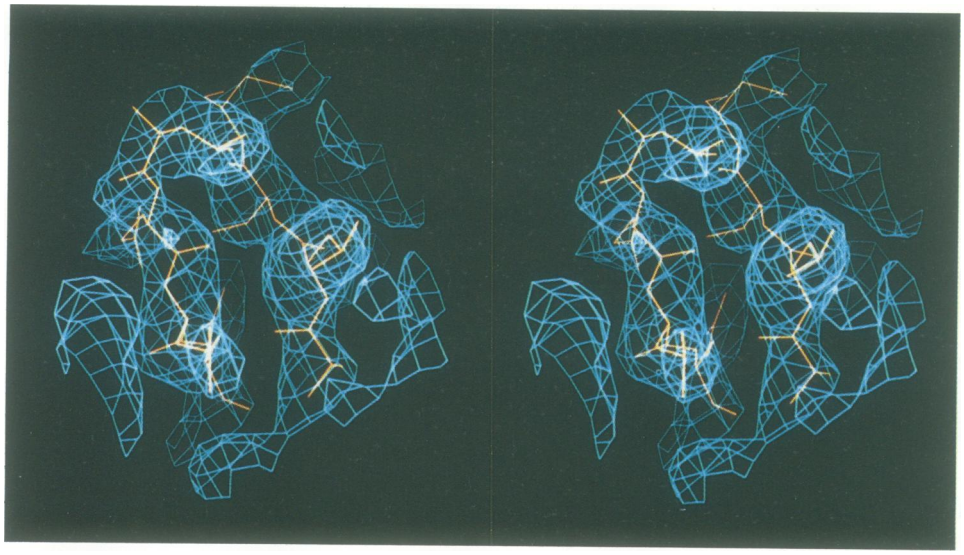

Fig. 1. Stereo picture of representative electron density at 3.0 Å resolution for IL-1β including the fitted model for parts of β-strands 6 (residues 68−71) and 7 (residues 80−83). The phases are derived from two heavy atom derivatives. Single derivative phases were improved individually by solvent flattening and the two phase sets were then combined. The electron density is contoured at one standard deviation above the mean.

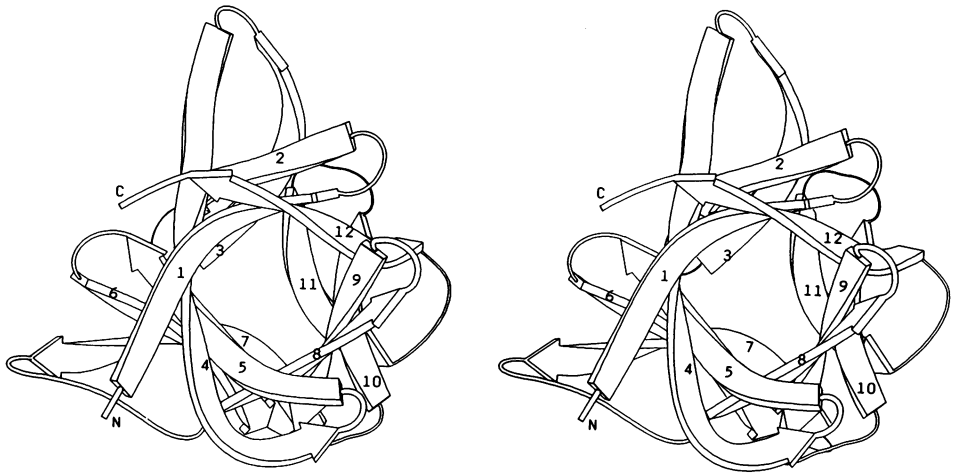

Fig. 2. Stereo cartoon (program written by J.P.P.) of IL-1β. The twisted arrows represent β-strands. They are numbered sequentially. The view is down the axis of the barrel formed by six of the β-strands.

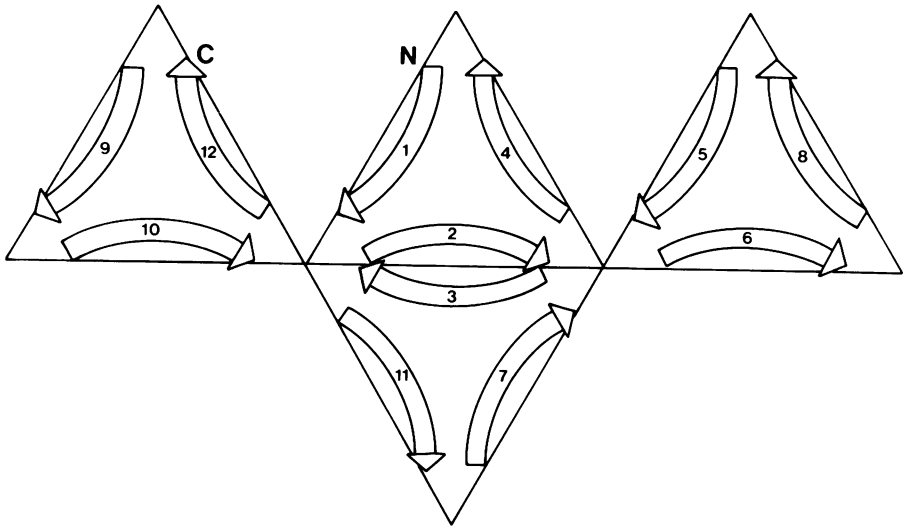

Fig. 3. Schematic drawing of the tetrahedron-like core of IL-1β with arrows representing the β-strands which are numbered as in Figure 2. For the sake of clarity, the loops connecting the β-strands have been left out. The tetrahedron has been opened up and laid flat. There is hydrogen-bonding along the full length of the edges of each face, but only near the vertices within the faces themselves.

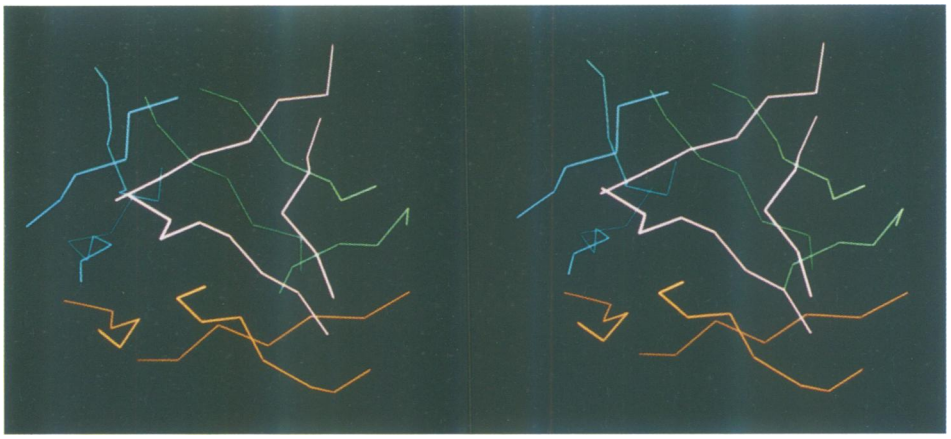

Fig. 4. Stereo C_α tracing of the tetrahedron-like core. Each of the four faces is coloured differently for clarity. The interior of this core is filled with hydrophobic side chains. Note the triangular arrangement of the three strands making up each face of the tetrahedron. The six-stranded barrel, at the top, is seen from a direction normal to its axis.

the fitted protein model. A subsequent electron density map after solvent flattening with the now known molecular envelope allowed most of the missing residues to be fitted. The final model prior to refinement gave a crystallographic *R*-factor of 42.3%.

Description of the structure

The most prominent features of the IL-1β structure are the β-sheet strands (Figure 2). Six of these form a barrel which is closed at one end by the other six strands. The overall folding is antiparallel β. It corresponds to an up-and-down β-barrel structure in the nomenclature of Richardson (1981). Other examples of this class include domain 2 of papain (Drenth *et al.*, 1971), domain 1 of catalase (Vainshtein *et al.*, 1986) and soybean trypsin inhibitor (Sweet *et al.*, 1974). The overall folding of IL-1β can be thought of as a distorted tetrahedron with openings at all of the vertices, one opening (the six-stranded barrel) being considerably larger than the others. Each triangular face of the tetrahedron is formed by three antiparallel β-strands which hydrogen-bond pairwise near the vertices, but not in the middle (Figure 3). The edges of the tetrahedron are formed by two anti-parallel β-strands, one on each adjoining face. Figure 4 is a C_α stereo picture of the 12 β-strands making up the core of the molecule.

A schematic drawing of the IL-1β structure is shown in Figure 5. It indicates a 3-fold internal structural pseudosymmetry. The overall folding of IL-1β is very similar to that found for soybean trypsin inhibitor, which also possesses 3-fold structural pseudosymmetry (McLachlan, 1979). For soybean trypsin inhibitor it was assumed that the 3-fold symmetry is due to gene triplication followed by gene fusion, although no internal sequence homology could be found. In IL-1β, the pseudo 3-fold axis gives rise to weak internal sequence homology between topologically corresponding residues. The only strong homology is found between β-strands 4 and 12 where four residues in a stretch of six are identical (Table I).

The interior of the molecule is strongly hydrophobic. Roughly two-thirds of the amino acid side chains filling this hydrophobic core are leucines and phenylalanines. There are no charged residues in the interior, where the only hydrophilic group is the phenolic hydroxyl group of a tyrosine, which does not appear to form a hydrogen bond. The

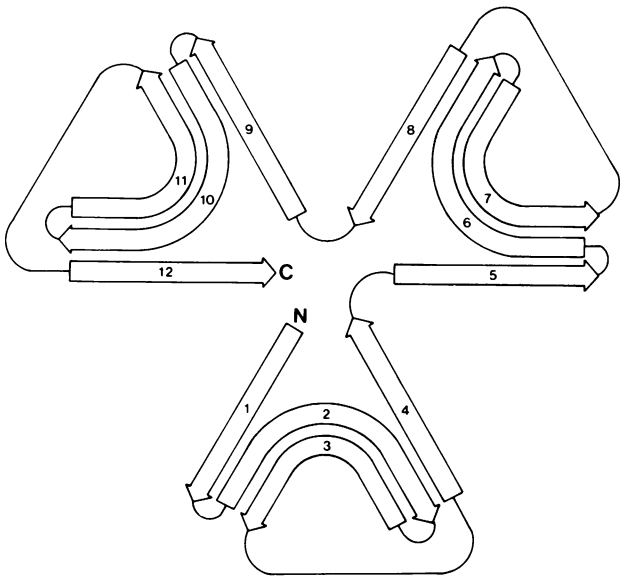

Fig. 5. Schematic drawing of the folding of IL-1β emphasizing the 3-fold pseudosymmetry of the secondary structure. The view is roughly the same as in Figure 2. β-Strands 1, 4, 5, 8, 9 and 12 form an antiparallel pleated sheet barrel at the 'front' of the molecule, which the remaining strands close at the 'back'. In three dimensions, β-strands 3, 7 and 11 are hydrogen-bonded to each other.

charged amino acid side chains are evenly distributed on the surface of the molecule.

The three-dimensional structure accounts for the observed spectroscopic and hydrodynamic properties of the molecule. The current model consists of about 65% β-sheet and 35% random coil/reverse turn. This is in good agreement with the CD results of Craig *et al.* (1987). Solvent perturbation spectroscopy (Wingfield *et al.*, 1987) shows the single tryptophan residue to be ~40% exposed to solvent. In the model, Trp-120 is indeed partially exposed. Wingfield *et al.* (1987) found the four tyrosines to be, on average, 50% exposed. In the model, one tyrosine is completely and two are partially exposed, while the fourth is completely buried. The overall shape of the molecule is roughly isometric, in correspondence with the f/f_o ratio of 1.09 from hydrodynamic studies (Wingfield *et al.*, 1986). Cys-71 does not react with the mercurial reagent PHMB. This can be

Table I. Sequence comparison of pseudo-3-fold related β-strands in IL-1β

Strand[a]	Sequence[b]										
1	V3	R4	S5	L6	**N7**	C8	T9	**L10**	R11	D12	
5		D54	K55	I56	P57	V58	A59	**L60**	G61	L62	
9					**N107**	N108	K109	**L110**	E111	F112	E113
2		Q15	K16	S17	**L18**	V19	M20	S21	G22		
6	K65	N66	L67	Y68	**L69**	S70	C71	V72	L73	K74	
10		P118	N119	W120	Y121	I122	S123	T124			
3			E25	**L26**	K27	A28	L29	H30	L31	Q32	G33
7	K77	P78	T79	**L80**	Q81	**L82**	E83	S84	V85	D86	P87
11		M130	P131	V132	F133	**L134**	G135	G136			
4	Q38	Q39	V40	V41	**F42**	S43	**M44**	S45	**F46**	**V47**	Q48
8			K97	R98	**F99**	V100	F101	N102	K103	I104	
12	D142	I143	T144	D145	**F146**	T147	**M148**	Q149	**F150**	**V151**	S152

[a]β-strands are numbered sequentially as in Figure 2.
[b]Identical residues in topologically identical positions are given in boldface. The sequence similarity in strands 4 and 12 is striking. No significant homology is found elsewhere.

understood from the model since it is not solvent accessible. The sole histidine residue (His-30) is on the surface of the molecule, but in the crystal access is prevented by a symmetry related molecule, explaining why it could not be labelled with heavy atom reagents such as K_2PtCl_4.

For the future, we plan to collect high-resolution data (2.0 Å) by oscillation photography and we will use this data to refine the structure.

Materials and methods

Crystallization

Human recombinant IL-1β of high purity was obtained from Biogen Ltd (Geneva). Crystals of IL-1β were grown from ammonium sulphate solutions by the hanging drop method as described by Schär *et al.* (1987). The crystals are tetragonal bipyramids which grow to maximum size (typically 1.0 × 1.0 × 1.2 mm^3) in 5–6 weeks and belong to space group $P4_1$ (or $P4_3$) with unit cell dimensions $a = b = 54.9$ Å, $c = 76.8$ Å. The same crystal form has been obtained by Gilliland *et al.* (1987) of human recombinant IL-1β obtained from Otsuka Pharmaceutical Company Ltd (Tokushima, Japan). The unit cell could accommodate (Matthews, 1968) either one (V_m = 3.33 $Å^3$/Da) or two (V_m = 1.66 $Å^3$/Da) molecules per asymmetric unit. The first low resolution electron density map resolved this ambiguity (see Results).

Data collection and data processing

Diffraction data were collected on a CAD4F diffractometer (Enraf–Nonius, Delft, The Netherlands) controlled by a VAX 11/730 computer. A cool air device (designed and built at the Biocenter) maintained the crystal temperature at about 4°C. An ω-scan of 0.5–0.7° (depending on crystal mosaicity) was used to collect the diffraction data. A statistical procedure was used to analyse the peak profile (M.Glor, unpublished results). Seven strong reflections were measured every two X-ray exposure hours to monitor intensity decay due to radiation damage. Data collection was stopped when ~15% decay had occurred, typically after about 30 h of exposure. There was no noticeable difference between the intensity decay rates of derivative as compared to native protein crystals. On average, about 3000 reflections per crystal could be recorded. A second order polynomial was fitted to the decay curve and used to correct for the time-dependent radiation decay. Anisotropic crystal absorption was corrected by the empirical method of North *et al.* (1968). Corrections for Lorentz and polarization effects were also made during the data reduction procedure. Baysian statistics were applied to determine the best intensity estimate of very weak reflections (French and Wilson, 1978). Multiple crystal data sets were scaled together by the method of Fox and Holmes (1966), using a standard set of 75 strong reflections evenly distributed throughout the resolution range 20–3.0 Å. Table II summarizes the data collection results.

Heavy atom derivatives

Potential heavy atom derivatives were prepared by soaking native IL-1β crystals in a stabilizing solution consisting of 50% ammonium sulphate (w/v) in 25 mM Tris–HCl buffer, pH 7.0, to which the appropriate heavy atom compound had been added. A low resolution (3.5 Å) data set was collected by diffractometry as described above and fitted to the native data by a least squares procedure that refines both overall scale and relative temperature factors. Difference Patterson maps were used to check for heavy atom binding. This procedure yielded two promising derivatives, PHMB and $UO_2(NO_3)_2$. Diffraction data for these derivatives were collected to

Table II. Native and derivative data collection statistics

	Native	PHMB	$UO_2(NO_3)_2$
Concentration	–	saturated	10 mM
Soaking time	–	12–14 h	10–11 days
Resolution (Å)	3.0	3.0	3.0
Number of crystals used	3	3	2
R-merge[a] (%)	7.1	9.5	6.2
R-factor[b] versus native (%)	–	14.5	25.1
Cullis *R*-factor[c] (%)	–	52.4	47.2

[a]$R\text{-merge} = \dfrac{\Sigma\,|\,<I(\mathrm{hkl})> - I(\mathrm{hkl})_i\,|}{\Sigma\,<I(\mathrm{hkl})>}$ for measurements from different crystals (i).

[b]$R\text{-factor} = \dfrac{\Sigma\,|F(\mathrm{hkl})_D - F(\mathrm{hkl})_N|}{\Sigma F(\mathrm{hkl})_N}$

where $F(\mathrm{hkl})_D$ and $F(\mathrm{hkl})_N$ are the derivative and native structure factor amplitudes, respectively.

[c]$\text{Cullis } R\text{-factor} = \dfrac{\Sigma\,|f_{h(obs)} - f_{h(calc)}|}{\Sigma f_{h(obs)}}$

where $f_{h(obs)}$ and $f_{h(calc)}$ are the observed and calculated heavy atom structure factor amplitudes, respectively, for centric data.

Table III. Heavy Atom parameters after refinement

Derivative	Site	Occ.[a]	*x*[b]	*y*	*z*	*B*	Binding
PHMB	1	9.2	0.197	0.389	0.100	20.0	Cys-8
	2	4.9	0.229	0.362	0.062	30.0	Cys-8
$UO_2(NO_3)_2$	1	11.6	0.143	0.150	0.236	0.0	Glu-64 Asp-35[c]
	2	10.6	0.294	0.448	−0.117	10.0	Asp-145

[a]In arbitrary units
[b]*x*, *y* and *z* are the fractional atomic coordinates, *B* is the atomic temperature factor in $Å^2$.
[c]Symmetry related molecule, i.e. binding is between two different IL-1β molecules.

Table IV. Mean figures-of-merit versus resolution

Phases	15.0–4.5 Å	4.5–3.5 Å	3.5–3.0 Å	Overall
(1) UO_2 SIR[a]	0.392	0.296	0.223	0.309
(2) PHMB SIR	0.362	0.192	0.141	0.237
(3) UO_2+SolFlat[b]	0.774	0.737	0.725	0.746
(4) PHMB+SolFlat	0.735	0.681	0.672	0.697
(5) Combined	0.840	0.786	0.776	0.803

Average phase difference between 3 and 4: 65.2°
Average phase difference between 3 and 5: 29.0°
Average phase difference between 4 and 5: 36.2°

[a]SIR = Single isomorphous replacement.
[b]Phases after solvent flattening.

3.0 Å. PHMB appeared to be a single site derivative while UO_2^{2+} binds at two sites. The x and y coordinates of the sites were determined from the Harker section $w=1/2$. The z coordinate of the single PHMB site was given the arbitrary value of 0.1 to fix the origin along the crystallographic z-axis, which is not defined by symmetry in $P4_1$ (or $P4_3$). The heavy atom coordinates x and y, the occupancy and the atomic temperature factor (B), as well as the overall scale factor and relative temperature factor were refined using only centric data (hk0) (Rossmann, 1960). An unusual feature was a very large B for the mercury site. The z coordinates of the two uranyl sites were determined from a difference Fourier map calculated with the single isomorphous replacement (SIR) phases from the PHMB derivative. Again the heavy atom parameters were refined using only centric data. The z-coordinates were refined by the method of phase refinement (Dickerson *et al.*, 1968) using the PHMB SIR phases. As a check, a difference Fourier map of the PHMB derivative was calculated using the uranyl SIR phases. From the difference Fourier map it became clear that there were actually two sites near each other for the PHMB derivative. This accounted for the large apparent temperature factor. These two sites were again refined using the centric data and the z-coordinate of the minor site was refined by phase refinement using the uranyl SIR phases. Table III gives the refined heavy atom parameters. Once tentative native phases had been determined from these two good heavy atom derivatives, difference Fourier maps were used to recheck potential derivatives which had not been solved by difference Patterson techniques. No additional useful derivatives were found, however.

Phase calculation and phase improvement

Native multiple isomorphous replacement (MIR) phases were calculated (Blow and Crick, 1959) using the PHMB and uranyl derivative data. All electron density maps were calculated with a grid spacing of approximately one-third the maximum resolution. A 5.0 Å electron density map was calculated and plotted onto transparent sheets. This map showed that there is one molecule per asymmetric unit, implying a crystal solvent content of ~63% by volume. This large solvent volume made it attractive to try to solve the phase ambiguity of the separate derivatives by solvent flattening. The solvent flattening and automatic protein–solvent boundary determination methods of Wang (1985) were applied to each derivative in turn. To ensure that none of the protein would be mistaken for solvent and subsequently be flattened, the solvent volume in the crystal was set to be only 50%. The phases derived by this procedure were then combined by the method of Hendrickson and Lattman (1970). These combined improved SIR phases were better than those obtained by the usual MIR procedure followed by solvent flattening, as demonstrated by the average figures-of-merit (0.80 versus 0.75) and confirmed by inspection of the respective electron density maps. Table IV shows the improvement of the figures-of-merit by this procedure. Examination of the electron density map showed the twist of the β-sheets (when viewed normal to the strands) to be right-handed, implying that the space group was incorrect and should be the enantiomorph $P4_3$ instead of $P4_1$. The heavy atom z-coordinates were inverted around $z = 0.1$ (to maintain the z-coordinate of the PHMB major site) and new phases and a new 3.0 Å electron density map for space group $P4_3$ were calculated.

Acknowledgements

The authors wish to express their thanks to Prof. J.N.Jansonius, in whose laboratory most of this work was carried out, for his interest and support.

References

Auron,P.E., Webb,A.C., Rosenwasser,L.J., Mucci,S.F., Rich,A., Wolff,S.M. and Dinarello,C.A. (1984) *Proc. Natl. Acad. Sci. USA*, **81**, 7907–7911.
Blow,D.M. and Crick,F.H.C. (1959) *Acta Crystallogr.*, **12**, 794–802.
Cameron,P., Limjuco,G., Rodkey,J., Bennett,C. and Schmidt,J.A. (1985) *J. Exp. Med.*, **162**, 790–801.
Craig,S., Schmeissner,U., Wingfield,P. and Pain,R.H. (1987) *Biochemistry*, **26**, 3570–3576.
Dewhirst,F.E., Stashenko,P.P., Mole,J.E. and Tsurumachi,T. (1985) *J. Immunol.*, **135**, 2562–2568.
Dickerson,R.E., Weinzierl,J.E. and Palmer,R.A. (1968) *Acta Crystallogr. B*, **24**, 997–1003.
Drenth,J., Jansonius,J.N., Koekoek,R. and Wolthers,B.G. (1971) *Adv. Prot. Chem.*, **25**, 79–115.
Fox,G.C. and Holmes,K.C. (1966) *Acta Crystallogr.*, **20**, 886–891.
French,S. and Wilson,K. (1978) *Acta Crystallogr. A*, **34**, 517–525.
Gery,I. and Lepe-Zuniga,J.L. (1983) *Lymphokines*, **9**, 109–126.
Gilliland,G.L., Winborne,E.L., Masui,Y. and Hirai,Y. (1987) *J. Biol. Chem.*, **262**, 12323–12324.
Hendrickson,W.A. and Lattman,E.E. (1970) *Acta Crystallogr. B*, **26**, 136–143.
Kronheim,S.R., March,C.J., Erb,S.K., Conlon,P.J., Mochizuki,D.Y. and Hopp,T.P. (1985) *J. Exp. Med.*, **161**, 490–502.
McLachlan,A.D. (1979) *J. Mol. Biol.*, **133**, 557–563.
March,C.J., Mosley,B., Larsen,A., Cerretti,D.P., Braedt,G., Price,V., Gillis,S., Henney,C.S., Kronheim,S.R., Grabstein,K., Conlon,P.J., Hopp,T.P. and Cosman,D. (1985) *Nature*, **315**, 641–647.
Matthews,B.W. (1968) *J. Mol. Biol.*, **33**, 491–497.
Mizel,S.B. and Farrar,J.J. (1979) *Cell. Immunol.*, **48**, 433–436.
North,A.C.T., Phillips,D.C. and Mathews,F.S. (1968) *Acta Crystallogr. A*, **24**, 351–359.
Oppenheim,J.J., Kovacs,E.J., Matsushima,K. and Durum,S.K. (1986) *Immunology Today*, **7**, 45–56.
Richardson,J.S. (1981) *Adv. Prot. Chem.*, **34**, 167–339.
Rossmann,M.G. (1960) *Acta Crystallogr.*, **13**, 221–226.
Schär,H.-P., Priestle,J.P. and Grütter,M. (1987) *J. Biol. Chem.*, **262**, 13724–13725.
Sweet,R.M., Wright,H.T., Janin,J., Chothia,C.H. and Blow,D.M. (1974) *Biochemistry*, **13**, 4212–4228.
Vainshtein,B.K., Melik-Adamyan,W.R., Barynin,V.V., Vagin,A.A., Grebenko,A.I., Borisov,V.V., Bartels,K.S., Fita,I. and Rossmann,M.G. (1986) *J. Mol. Biol.*, **188**, 49–61.
Wang,B.-C. (1985) *Methods Enzymol.*, **115**, 90–112.
Wingfield,P., Payton,M., Graber,P., Rose,K., Dayer,J.-M., Shaw,A.R. and Schmeissner,U. (1987) *Eur. J. Biochem.*, **165**, 537–541.
Wingfield,P., Payton,M., Tavernier,J., Barnes,M., Shaw,A., Rose,K., Simona,M.G., Demczuk,S., Williamson,K. and Dayer,J.-M. (1986) *Eur. J. Biochem.*, **160**, 491–497.

Received on November 2, 1987; revised on November 30, 1987

Note added in proof

The structure has been improved by crystallographic least-squres refinement using data to a resolution of 2.6 Å and has a crystallographic R-factor of 18.8%. The structure as described here has been confirmed.